JOURNAL OF Materials CHEMISTRY

Synthesis of zinc oxide nanoparticles with controlled morphology

Lingna Wang and Mamoun Muhammed*

Materials Chemistry Division, Royal Institute of Technology, SE-100 44 Stockholm, Sweden. E-mail: mamoun@matchem.kth.se

Received 12th May 1999, Accepted 6th September 1999

A chemical precipitation method has been used for the synthesis of ZnO nanoparticles with controlled morphology. The precursor powders were prepared using several precipitation reagents and using ammonium carbamate as a precipitating reagent led to unusual rod-shape morphology. The precursor was decomposed by heating in air resulting in the formation of spherical or rod-like shapes of zinc oxide. A flow injection synthesis technique has been developed to synthesize nanophase particles of zinc oxide. The precursor and decomposed products were analyzed using IR, SEM, XRD and TGA techniques. The average size of the particles of ZnO obtained using the flow injection technique was approximately 20 nm while the crystallite size as measured from the X-ray pattern was 10–15 nm.

Zinc oxide has a broad range of applications, *e.g.*, in pigments, rubber additives, gas sensors, varistors and transducers.[1] Several studies on the fabrication of mixed metal oxides containing ZnO have been reported. The studies were carried out in order to fine-tune ZnO properties for special applications. It has recently been demonstrated that nanophase zinc oxide can be used in photocells of the Grätzel type,[2] which results in improved current generation efficiency. Zinc oxide with a particle size in the range 100–200 nm has proved to be an excellent UV absorbing material, which can be used in sunscreen lotions to enhance the sun protection factor.[3] Pure zinc oxide is an insulator and improving its conductivity extends its use to many new applications. Zinc oxide with increased conductivity is suited for applications where static charge build-up must be prevented. The electrical conductivity can be significantly increased by doping or the introduction of defects into the ZnO crystal lattice, which can improve the electrical conductivity to the high end for semiconductors. In conventional powder metallurgy, the use of ultrafine zinc oxide powder has significant advantages; *e.g.*, it lowers the sintering temperature. Moreover, a smaller grain size leads to an increased density of the sintered materials.

Nanophase materials have been prepared using physical methods, *e.g.*, gas evaporation.[4] Chemical methods have shown several distinct advantages for the synthesis of nanophase particles.[5] Several chemical methods for the manufacture of zinc oxide and mixed metal oxides have been reported, *e.g.*, preparation of fine zinc oxide by means of spray pyrolysis;[6] sol–gel technique[7–9] and thermal decomposition.[10] The synthesis of zinc oxide from organic solutions has also been reported, *e.g.* precipitation from alcohols and amines.[11–13] In some of these studies, the control of particle morphology and the rate of particle growth have been considered in order to avoid the formation of large particles. However, for nanophase powders, morphology manipulation and the preparation of unaggregated particles have received much less attention. Different synthesis techniques and appropriate reagents for the chemical control of nanophase particles with distinct shapes still present major challenges in this field.

Chemical methods, including precipitation from inorganic or organic solutions and sol–gel techniques can conveniently provide control of nucleation, growth and ageing of particles in the solution. The methods rely on advanced solution and coordination chemistry theories enabling the synthesis of the required precursor particles utilizing a variety of parameters to enable control of the solid formation process. A major contribution to the growth of particles is through Ostwald ripening, where small particles with lower solubility product dissolve and re-precipitate on the surface of larger particles in solution. Agglomeration takes place in solution as the particles clog together to minimize surface energy.

These processes are especially important when the precipitation takes place in solution where particles have free access to each other. In order to minimize or eliminate this access, the precipitation reaction should take place in confined zones separated from each other rather than in the bulk solution. A microemulsion can be made to contain aqueous droplets as the dispersed phase separated from each other by the continuous organic phase. In such a system, it is possible to carry out the precipitation in the confined water droplets.[14,15] In the microemulsion system, the extent of particle growth is reduced because precipitation occurs in the isotropic solution of the microdroplets (10–100 nm in diameter) which are surrounded by the continuous phase. In this way, particle growth, due to the interaction between different aqueous solutions, can be inhibited and very small sized particles are formed.[14] Another way to carry out the reaction within a confined volume is through the use of a set-up similar to that of flow injection analysis. In this paper, several approaches describing the synthesis of zinc oxide powder in solution and in confined zones are investigated.

Experimental

Reagents

Analytical grade reagents; $ZnCl_2$ and $NH_2CO_2NH_4$ (MERCK) of at least 99% purity were used as received without further purification. Stock solutions of $ZnCl_2$ and $NH_2CO_2NH_4$ were prepared by the dissolution of the appropriate amount of each salt in distilled water.

Bulk synthesis

The synthesis of ZnO precursors was carried out using chemical precipitation. Solutions of $ZnCl_2$ and $NH_2CO_2NH_4$ were simultaneously mixed under stirring until the precipitation was complete; gas evolved from the solution during the reaction. The solutions were filtered and the resulting solids were washed with distilled water several times until no chloride was detected in the filtered water (checking with Ag^+ solution). The precipitates were then dried at 105 °C in an oven overnight.

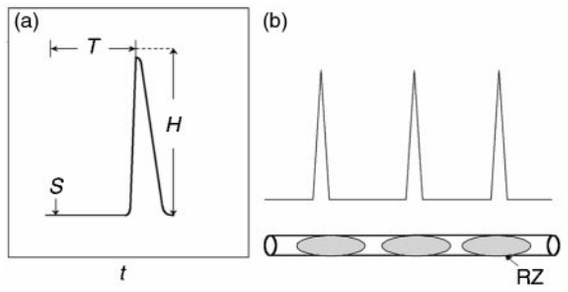

Fig. 1 (a) A typical FIA peak from recorder output (*S*, sample injection; *H*, peak height; *T*, residence time); (b) a schematic representation of confined reaction zone in the carrier stream (RZ, reaction zone).

ZnO with a slightly yellow colour was obtained after calcination of the precipitates in air at 350 °C for 3 h.

Synthesis in a confined zone

The flow injection analysis (FIA) method has been widely applied in the area of analytical chemistry.[16–18] FIA is an automated microchemical technique having a high sampling rate and capable of controlling the dispersion of the sample zone with minimum reagent consumption. The technique is based on the injection of a liquid sample into a moving, non-segmented continuous carrier stream of suitable liquid. The FIA system is based on three principles: sample injection, reproducible timing and controlled dispersion. Analytical applications of FIA include colorimetric detection in which a reaction is carried out in a confined segment, between the required component and added reagents, to form a product complex or species that can be detected continuously by a suitable detector. A typical recorded output has the form of a peak [Fig. 1(a)] the height (*H*) of which is proportional to the concentration of the species. This indicates that the reaction is confined to a limited volume of the carrier stream. The time span between the sample injection (*S*) and the peak maximum, which yields the analytical readout, is the residence time (*T*) during which the chemical reaction takes place. The controlled dispersion of the sample zone which occurs during its passage through the system towards the detector results in a response curve, the peak shape of which is characteristic of the FIA system. By changing the flow parameters, the dispersion can be manipulated easily to suit the requirements of a particular chemical procedure so that an optimum response is obtained for the shortest time and minimum amount of reagent.

Flow injection analysis can be modified and applied to carry out reactions for the formation of solid particles. A flow injection manifold can be designed in which the different reactants can be injected into a given reaction zone [RZ in Fig. 1(b)]. The reaction conditions in each zone, separated by the carrier solution, can be easily adjusted to those required for the precipitation reaction. Subsequent additions of the reactants can be performed after time *T*, which results in a subsequent separate reaction zone. In this case, Ostwald ripening can only take place through the interaction between particles within the same zone and not between particles existing in different zones. By careful selection of the reactant and mixing inside each reaction zone, particle growth can be significantly reduced. Moreover, more uniform size particles can be produced in this way.

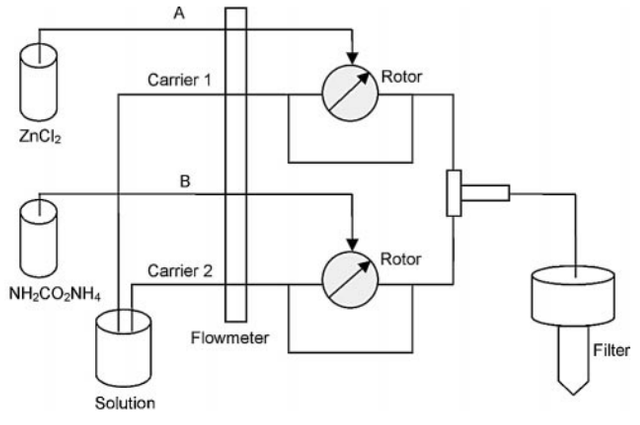

Fig. 2 A schematic representation of the FIS system used in the current study.

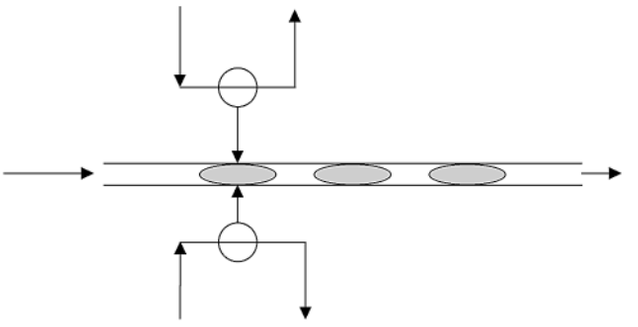

Fig. 3 The synchronous merging of two zones in an FIS system.

Flow injection synthesis (FIS)

A schematic diagram of the FIS system is shown in Fig. 2. Zinc chloride and ammonium carbamate solutions are pumped from individual containers into the system at predetermined time intervals. This causes the flowing stream to be regularly segmented by the solutions A and B. Carrier streams 1 and 2 are pumped at equal rates *via* lines x and y through tubes of equal length. By using two-injection valves, solutions containing the different reactants A and B are introduced into the cavities of the rotor, the length and internal diameter of which determine the solution volume. While in the reactant injection position, the carrier stream is shut through a bypass. After turning the rotor to the inject position, a precise volume of reactant-containing solution is swept along by the carrier stream into the system, because the bypass has a higher hydrodynamic flow resistance than does the solution path. The purpose of using a valve is to inject solution into the reaction zone that moves along with the carrier streams pumped at the same speed, and mixed in a controlled manner as shown in Fig. 3.

A synchronized merging of the two solutions takes place in a symmetrical system with continuous pumping where equal volumes of zinc solution and precipitating solutions are

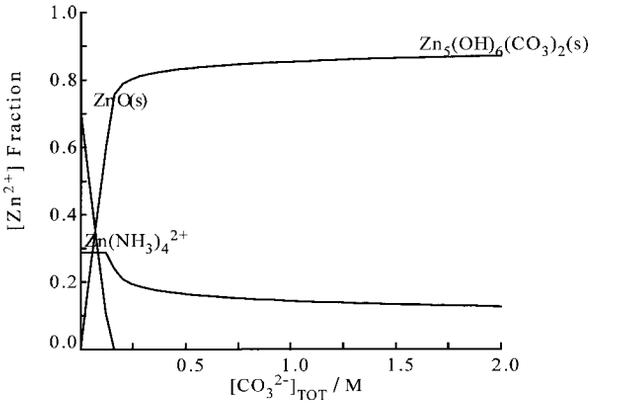

Fig. 4 Thermodynamic calculation on the system $Zn–NH_3–CO_3^{2-}$ showing the effect of concentration of carbonates on the formation of different zinc species at pH = 10.

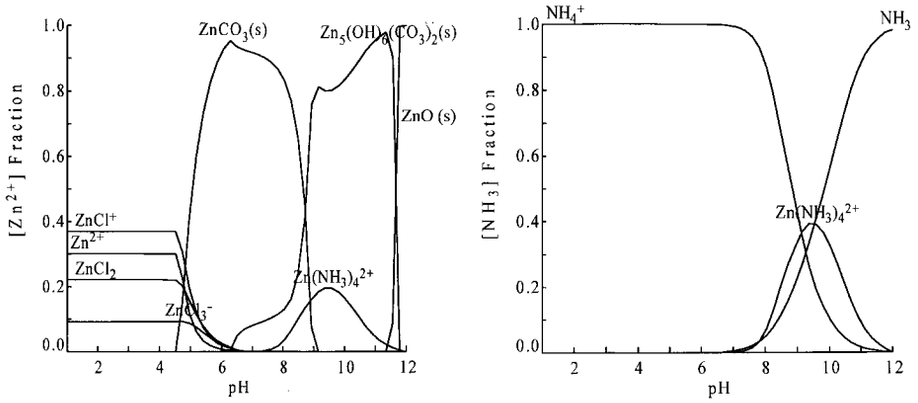

Fig. 5 Distribution of different zinc species at various pH regions calculated for the system Zn–NH_3–CO_3^{2-}.

injected and combined at identical velocities. After passing through equal lengths of tubing downstream the solutions continue to react and precipitates are thus formed. The precipitates are then separated from the solution by filtration. The following steps of drying and calcination are similar to those of the bulk synthesis.

Results and discussion

Zinc ions are appreciably hydrolyzed, because of the ability of the Zn^{2+} ion to increase its coordination number above four, to form different species such as $[Zn(OH)(H_2O)_x]^+$ and $[Zn_2(OH)(H_2O)_x]^{3+}$ and a number of basic hydroxo-salts such as $ZnCO_3{\cdot}2Zn(OH)_2{\cdot}H_2O$ which can be precipitated.[19] Polynuclear hydroxy carbonate species such as $Zn_5(OH)_6(CO_3)_2$ can also be precipitated from zinc ions in solution at moderate Zn^{2+} concentration, pH and carbonate concentrations. $Zn_5(OH)_6(CO_3)_2$ is reported to be a stable phase in the presence of atmospheric CO_2(g).[20,21] Equilibrium calculations have been used to examine the different conditions for the formation of precipitates and complexes. The reaction between zinc and carbamate can lead to different zinc compounds; *e.g.* carbonate, hydroxycarbonate or other complexes, whose composition depends on the pH range.

Ammonium carbamate which is used as a precipitating reagent, is an ester salt of carbamic acid (NH_2CO_2H). Carbamic acid itself and N-substituted derivatives of carbamic acid are unstable and decompose spontaneously to carbon dioxide and ammonia or an amine, while carbamates are relatively stable.[22] The concentrations of carbonate and ammonia are controlled by the decomposition of ammonium carbamate. Zinc precipitates are significantly affected by the concentration of carbonate and ammonia resulting from ammonium carbamate. As can be seen in Fig. 4, two solid species, ZnO and $Zn_5(OH)_6(CO_3)_2$, are formed at different concentration regions of carbonate around pH = 10. $ZnCO_3$ does not form at pH = 10, while $Zn_5(OH)_6(CO_3)_2$ is the predominant precipitate when the carbonate concentration is above 0.3 M.

Fig. 5(left) shows that $ZnCO_3$ can be formed in the pH region 5–9 depending on the concentration of carbonate, while the $Zn_5(OH)_6(CO_3)_2$ precipitate forms in the pH region 6.5–11.5. Zinc chloride complexes are relatively weak and are of importance only at fairly high chloride concentrations. The $Zn(NH_3)_4^{2+}$ complex cation forms in the pH region 7–12 as shown in Fig. 5(right).

The reaction of zinc ions and ammonium carbamate proceeds according to eqn. (1):

$$5ZnCl_2 + 5NH_2CO_2NH_4 + 8H_2O \rightleftharpoons Zn_5(OH)_6(CO_3)_2(s) + 3CO_2(g) + 10NH_4Cl \quad (1)$$

The solid precipitate which forms decomposes upon calcination to ZnO [eqn. (2)]

$$Zn_5(OH)_6(CO_3)_2(s) \rightarrow 5ZnO + 2CO_2 + 3H_2O \quad (2)$$

A series of experiments was performed in order to investigate the effect of varying the ammonium carbamate concentration in the synthesis on the yield of zinc oxide precursor precipitate. The results (Fig. 6) show that, for 1 M zinc chloride solution, the maximum precipitation yield was about 83% at an ammonium carbamate concentration of 1.1 M.

A further increase in the concentration of ammonium carbamate did not increase the precipitation yield. This can be explained by the formation of zinc–ammonia complexes as shown by the equilibrium calculations in Fig. 7, where *ca.* 20% of the zinc ions react with ammonia to form the soluble $Zn(NH_3)_4^{2+}$ complex. The pH range for the preparation of $Zn_5(OH)_6(CO_3)_2$ was estimated to be between 9 and 11.5.

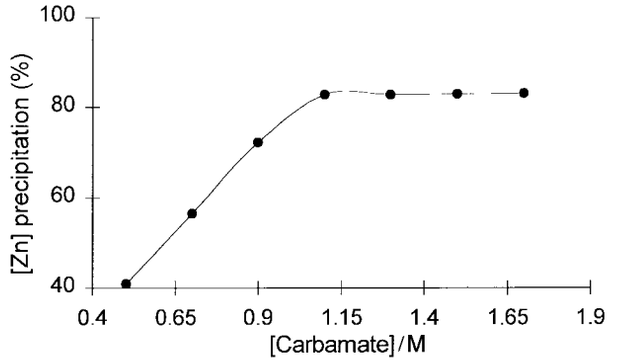

Fig. 6 Effect of the concentration of ammonium carbamate on the precipitation of the zinc oxide precursor at pH = 10.

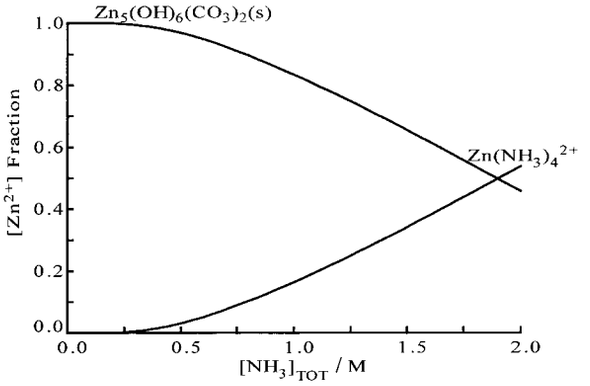

Fig. 7 Thermodynamic calculation on the system Zn–NH_3–CO_3^{2-} showing the effect of concentration of ammonia on the formation of different zinc species at pH = 10.

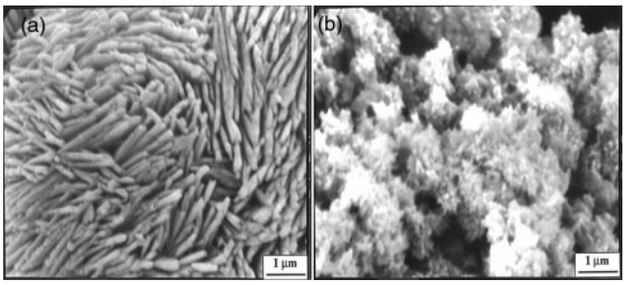

Fig. 8 SEM photographs of the zinc oxide precursor (pH 10, $NH_2CO_2NH_4$, FIS): (a) dried sample, (b) sample prior to drying.

The precipitation was carried out at pH 10 which is favourable for the formation of the $Zn_5(OH)_6(CO_3)_2$ species. Characterization of the powders before calcination was investigated using a scanning electron microscope (SEM). The dried powder [Fig. 8(a)] was nanosized and had a different morphology from the as-precipitated powder [Fig. 8(b)]. The as-precipitated powder contained *ca.* 60–70 wt% water, while the dried powder contained <2 wt% water after drying in an oven at 100 °C for several hours.

X-Ray diffraction data collected for the as-precipitated powder showed that all the peaks could be identified as reflections of the $Zn_5(OH)_6(CO_3)_2$ phase as shown in Fig. 9 (solid line). The dashed curve is the XRD pattern for the powder after calcination, which indicates complete decomposition of the precipitate to a single phase of zinc oxide.

Thermogravimetric analysis (TGA) was carried out to investigate the decomposition process of the zinc oxide precursor. As shown in Fig. 10, the first step of the thermal decomposition is the loss of water followed by the decomposition of the $Zn_5(OH)_6(CO_3)_2$ phase to ZnO, as seen from the weight loss. The observed weight loss of 26.0% agrees very well with the theoretical value of 25.9 wt% according to eqn. (2). Weight loss due to water removal was estimated to be *ca.* 1–2 wt%. Rapid decomposition of the powder takes place at *ca.* 270 °C, after which only slow decomposition takes place which may be the result of the decomposition of a small amount of zinc carbonate possibly formed upon drying the precipitate. A temperature as low as 300 °C is sufficient for complete decomposition of the precipitated zinc compound. The ZnO obtained after calcination at 350 °C for 3 h had a slightly yellowish colour.

Further investigation of the precipitates was carried out by IR spectroscopy (Perkin Elmer FT-IR Spectrometer 1725X). IR analysis was carried out on oven-dried samples. The as-precipitated samples could not be examined by this technique since they contained too much water. The sample for IR analysis (pH 10, $NH_2CO_2NH_4$) was prepared by mixing KBr

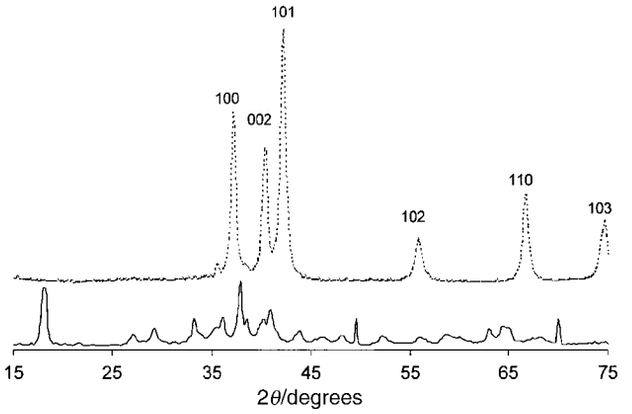

Fig. 9 XRD pattern for the as-precipitated powder (—) and the powder after calcination at 350 °C (···) showing the formation of pure ZnO.

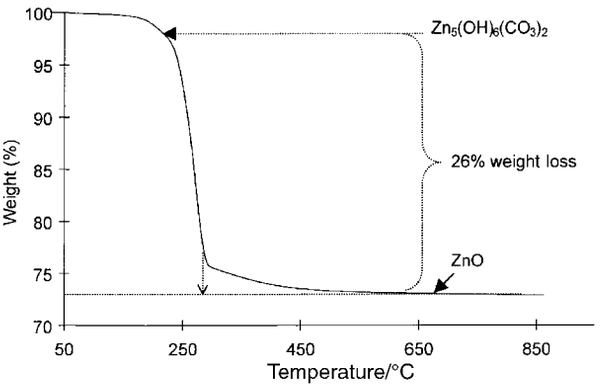

Fig. 10 Thermogravimetric analysis of decomposition of the zinc oxide precursor (pH 10, $NH_2CO_2NH_4$).

with 10 wt% ZnO powder and then pressing into a pellet *in vacuo* at 200 kg cm^{-2} for 1 min. Fig. 11 shows the resulting IR spectrum. As can be seen, there is a strong absorption peak at 1400–1300 cm^{-1} attributed to carbonate along with a medium stretch peak at 880–800 cm^{-1}.[23,24] There is another medium peak at 3500–3200 cm^{-1} arising from the hydroxy group, which when uncoordinated appears at *ca.* 3200 and 3700 cm^{-1}. These results suggest that hydroxy groups are coordinated to zinc ions. From Fig. 11, no evidence for NH_3 absorption in the IR spectrum can be seen. Fig. 12 shows the IR spectrum of the calcined powder and reveals significant changes in comparison with the sample before calcination. This can be attributed to the fact that zinc–hydroxy bonds are eliminated at 250 °C, as was indicated by the TGA analysis. No absorption peaks of hydroxy groups appear in the sample calcined at 350 °C and it is apparent that the precipitate had fully decomposed and the absorption peaks can be attributed solely to ZnO.

Effect of the zinc concentration

Thermodynamic calculations were used to study the effect of zinc concentration on the formation of precipitates. The formation of $Zn_5(OH)_6(CO_3)_2$ took place in the pH range 9–11.5 and became more predominant with increasing zinc concentration as shown in Fig. 13. On the other hand, high zinc concentrations increased the formation of agglomerates during the precipitation process.

Different concentrations of zinc solution were used to study the particle morphology. The shape and microstructure of particles are greatly affected by the concentration of zinc in solution. Fig. 14 shows SEM photomicrographs of various zinc precipitates prepared using different concentrations of zinc solution. The morphology and the size of the particles were different when zinc solutions of different concentrations were

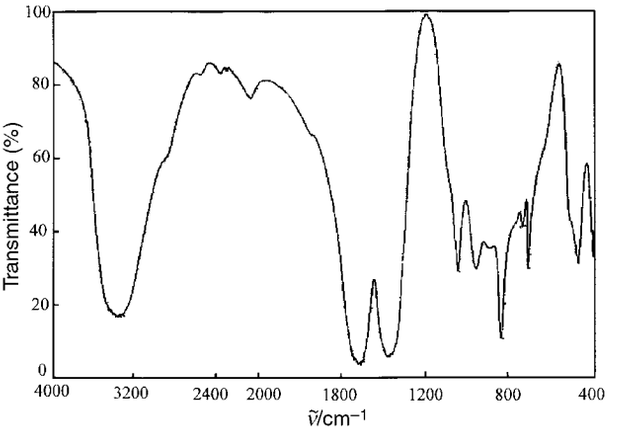

Fig. 11 IR spectrum of zinc oxide precursor (pH 10, $NH_2CO_2NH_4$).

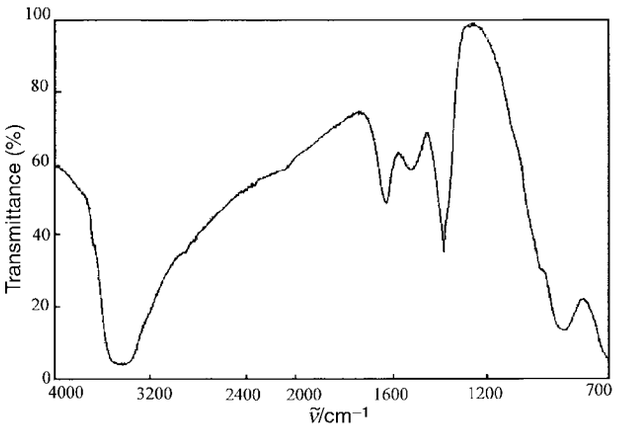

Fig. 12 IR spectrum of the zinc oxide precursor (pH 10, $NH_2CO_2NH_4$) after calcination at 350°C for 3 h.

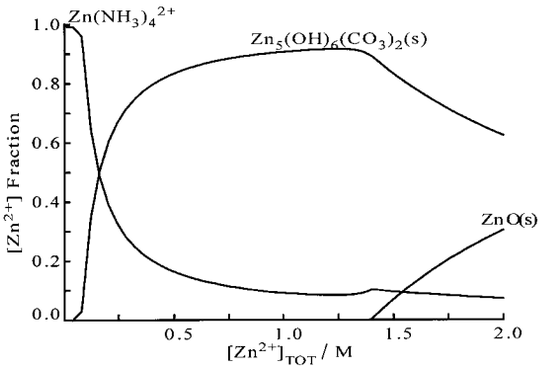

Fig. 13 The distribution of the different zinc species as calculated as a function of the total zinc concentration in the system $Zn–NH_3–CO_3^{2-}$ at pH = 10.

used (0.1–1 M $ZnCl_2$). The powder precipitated from 1 M Zn^{2+} solution consisted of plate-like grains with an average particle size of 0.5 μm whereas powder precipitated from 0.5 M Zn^{2+} solution consisted of needle-like grains ranging in length from 0.1 to 0.3 μm. The powder precipitated from 0.1 M Zn^{2+} solution consisted of needle-like grains ranging in length from 50 to 100 nm. At higher zinc concentrations, larger particles were formed with significant agglomeration. Using solutions with low Zn^{2+} concentration, led to more than one morphology, with rod-shaped nanosized particles, 10–20 nm in diameter, along with large spherical particles, similar to those shown in Fig. 14(c), which always co-existed when $C_{Zn^{2+}} < 0.1$ M. The smallest particles were formed at the lowest concentration of Zn^{2+} used. It seems, therefore, that at low concentrations of zinc, a high nucleation rate competes favourably with a lower growth rate of the already formed particles, allowing a large number of nucleations to take place before suitable environmental conditions allow the nuclei to grow.

Effect of precipitating reagents

The presence of ammonium seems to be important for the formation of particles with morphologies different from the sphere-shaped morphology commonly obtained in the absence of ammonia. From the thermodynamic calculations, the interaction of ammonium ions with Zn^{2+} seems to be limited and only *ca.* 20% of the zinc ions react with ammonia to form $Zn(NH_3)_4^{2+}$ species which are soluble (Fig. 6). Table 1 shows the ammonia concentration in the precipitated powders before and after drying as well as in the zinc oxide produced by the calcination of the powders.

As noted earlier, the water content in the as-precipitated powder is very high (60–70%) when the powder was air-dried. The total amount of NH_4^+ in the as-precipitated powder can be expressed by eqn. (3).

$$\Sigma \mathrm{mol}(NH_4^+)_{\mathrm{total}} = \mathrm{mol}(NH_4^+)_{\mathrm{solid}} + \mathrm{mol}(NH_4^+)_{\mathrm{solution}} \quad (3)$$

It is assumed that the concentration of NH_4^+ in the liquid bound to the precipitate is the same as that of the solution bulk. The concentration of NH_4^+ in the solution contained within the solid phase [eqn. (1)], as inferred from Table 1, is *ca.* 6.5×10^{-3} mol per gram of precipitate with *ca.* 1.2×10^{-3} mol per gram of precipitate being associated with the solid phase.

The presence of NH_4^+ in the precipitates can be explained in two ways: either they adsorb onto the surface of the particles or they chemically participate in the formation of the solid precipitate and are thus a part of the formed precipitate. The amount of NH_4^+ in the oven-dried sample was much lower than that of as-precipitated powder which may be a result of decomposition of NH_4Cl on the surface of the particles. It was also noted that the amount of NH_4^+ in the calcined sample was lower than in the dried sample, which was in agreement with the results of the IR spectroscopy. As $Zn_5(OH)_6(CO_3)_2$ was the only phase formed, it appears that ammonium ions were simply adsorbed on the surface of the particles. If it is assumed that ammonia was adsorbed as a monolayer on the surface of the particles, the concentration of ammonium would be *ca.* 6.64×10^{-18} mol of ammonia per particle. (Particle size and shape were determined by SEM.) The experimentally determined concentration gave the ammonia content as *ca.* 8.96×10^{-18} mol per particle, as calculated from Table 1. The adsorption of ammonia on the surface of the particles is supported by the results of Sherif and Via[25] who have shown that ammonium nitrate (NH_4NO_3), is adsorbed on the surface of powders after precipitation. It is therefore concluded that NH_4Cl is adsorbed onto the surface of the particles, probably owing to the high surface energy associated with the nanophase materials. After careful examination of the SEM micrographs, it appears that the rod-shaped particles consisted of several spherical particles aligned in one direction. Ammonium ions may form a monolayer on the surface of such particles and connect them together by H-bonding; *i.e.* ammonium ions may be responsible for the observed morphology.

To further investigate the role of the precipitating reagent, the precipitation of precursors for the synthesis of zinc oxide has been carried out using a variety of salts. SEM photographs (Fig. 15) show that the following compounds had an effect on the morphology of the particles; $H_2C_2O_4$ [Fig. 15(a)], $(NH_4)_2C_2O_4$ [Fig. 15(b)], $NH_4(HCO_3)$ [Fig. 15(c)], $NaHCO_3$ [Fig. 15(d)], $(NH_2)_2CO$ [Fig. 15(e)], NH_3(aq) [Fig. 15(f)] and NaOH [Fig. 15(g)], which led to different grain shapes of the precipitates.

Particles with different chemical composition have, as expected, different shapes and sizes [Fig. 15(b), (d), (e) and

Table 1 Ammonium ion content in the zinc oxide precursor (pH 10, $NH_2CO_2NH_4$, FIS) and zinc oxide after calcination

Sample	Water content (%)	NH_4^+/mg g^{-1}	NH_4^+/mol (g powder)$^{-1}$
As-precipitated powder	60–70	138	7.7×10^{-3}
Dried precipitated powder (100 °C, overnight)	≈1	0.97	5.4×10^{-5}
ZnO (350 °C, 3 h calcination)	<1	0.055	3.1×10^{-6}

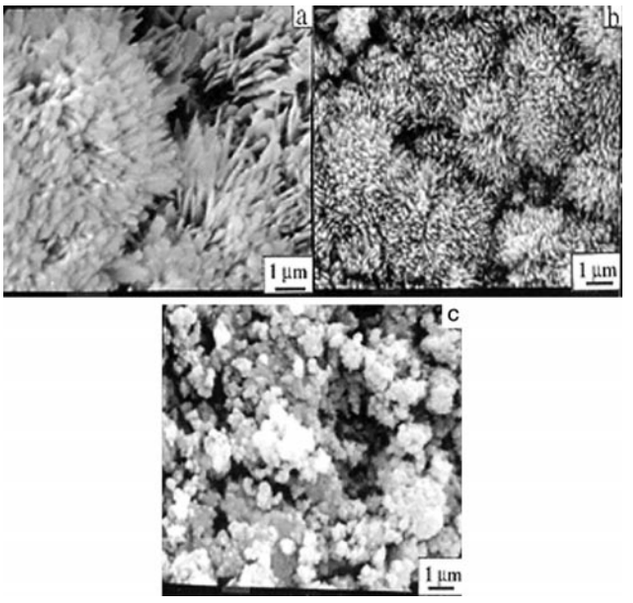

Fig. 14 SEM photographs of zinc oxide precursor precipitates prepared using different concentrations of Zn^{2+}: (a) 1 M; (b) 0.5 M; (c) 0.1 M.

(g)]. However, particles with the same chemical composition may have different morphology. From Fig. 15(a) and (b) it is evident that the precipitates formed in both cases have the same composition but different morphology. In both cases, the precipitates have the chemical composition ZnC_2O_4, but while the particles obtained from oxalic acid were of cubic shape with

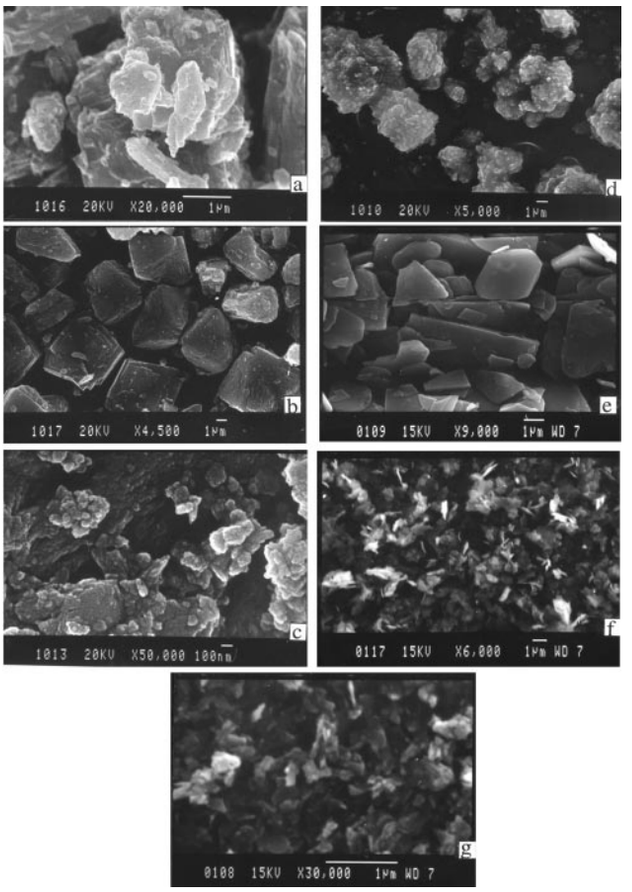

Fig. 15 SEM photographs showing different morphology of particles formed by the reaction of zinc chloride solution and different precipitating reagents: (a) $H_2C_2O_4$; (b) $(NH_4)_2C_2O_4$; (c) $NH_4(HCO_3)$; (d) $NaHCO_3$; (e) $(NH_2)_2CO$; (f) NH_3(aq); (g) NaOH.

an average particle size of 500 nm. Fig. 15(b) shows precipitates with different morphology produced *via* $NH_4(HC_2O_4)$. Likewise, $Zn(HCO_3)_2$ appeared to give rise to plate-like particles of a few μm in diameter [Fig. 15(c) and (d)], whereas the particle size of precipitates from $NH_4(HCO_3)$ was <100 nm.

The precipitation of $ZnCO_3$ from $(NH_2)_2CO$ solution was carried out at 80 °C, involving relatively slow reactions between Zn^{2+} and urea, resulting in the formation of large well faceted particles. It would appear that the morphology of the precipitates are thus strongly affected by different ligands. Differences also arise from the use of different cations even if the ligands are similar, *e.g.* particles being connected to each other in the presence of NH_4^+ ions, as cited earlier.

Effect of precipitation time

The reaction or residence time of the particles in the reaction media (mother-liquor) affected the size of the particles. There are three regimes in the generation of particles during the precipitation process. The first is the induction time, during which the reaction slowly generates the building units of the solid, still in solution. The second is the nucleation period, during which the concentration of the building units in solution builds up until a critical supersaturation level is reached and nucleation occurs. A relatively short nucleation period produces a narrow size distribution of nuclei and relieves the supersaturation to below the critical value, preventing further nucleation. After nucleation, during the third period, the growth proceeds until the reaction stops, *i.e.* when the concentrations of the reacting species in solution reach equilibrium. Nanoparticles in solution are very sensitive during this period and they grow as the residence time increases. Depending upon the rate-limiting step during growth, the particle size distribution may become narrower or remain constant as the particle growth proceeds.

The three regions can be defined in Fig. 16. The first region is the precipitation time of 0–2 min, which is the induction time (see insert in Fig. 16). In the second region, small particles (10–20 nm) are initially formed at shorter residence times of <10 min. During this time, the particle size rapidly increases and the initial growth rate in this region is *ca.* 2×10^{-4} μm s^{-1} (calculated from the data in Fig. 16). The growth rate is influenced by several mechanisms, of which Ostwald ripening is probably the most important. After *ca.* 10 min slow particle growth occurs at a much reduced level, *ca.* 1.5×10^{-5} μm s^{-1}, compared to that in the nucleation region. The particle size increases, up to 220 nm for a residence time of 125 min.

Synthesis using the FIS technique

The main advantage of the FIS technique is that the precipitation process is only allowed to continue for a limited

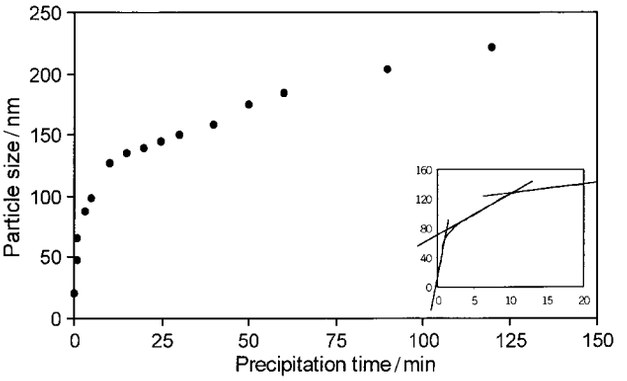

Fig. 16 The dependence of the particle size of the zinc oxide precursor on the reaction time.

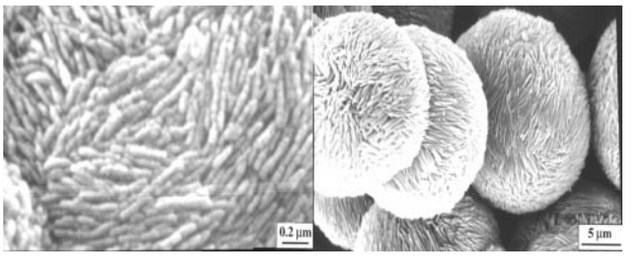

Fig. 17 SEM photographs of zinc oxide obtained through reaction in confined zones using FIS.

period of time of 1–2 min. The chemical reaction commences at the moment the solutions are mixed and the precipitation takes place and is complete in a confined zone. As shown in Fig. 2, the two reactants, zinc chloride and ammonium carbamate are injected simultaneously into the carrier stream, and mixed together. The precipitate formed has the same composition as that obtained in the bulk solution. The residence time is selected to allow completion of the reaction, after which the precipitates are passed through a tube to a suitable filter. Particles synthesised using the FIS technique have a residence time of only 1–2 min. In this way, the agglomeration is greatly limited, as the short residence time allows only primary nucleation. The subsequent mixing of solutions, A and B, is performed under reproducible conditions whereby powders with identical properties are obtained. The particles obtained from FIS have rod-shape morphology with size in the range 10–15 nm (Fig. 17). Powders obtained using FIS show only rod shape morphology whereas powders obtained from precipitation in bulk solution may contain particles of variable morphology.

Calcination of the zinc oxide precursor precipitate

Precursor precipitates were transformed into zinc oxide by thermal decomposition. Fig. 10 shows the TGA plot of the decomposition of a precipitate using carbamate as the precipitating reagent. Decomposition took place in one step to form zinc oxide at *ca.* 270 °C. TGA plots of precipitates obtained from the bulk solution and from FIS are similar. However, the precipitates obtained by FIS had a smaller particle size and required shorter calcination times in comparison to precipitates obtained from bulk solution synthesis. The calcined ZnO particles derived from the FIS technique were also smaller than those obtained by precipitation in non-confined zones.

The particle size of calcined ZnO powders were very sensitive to the calcination time. Fig. 18 shows that the specific surface area of particles decreased with increasing calcination time. The longer the calcination time, the larger the particle size of the ZnO powder produced. In addition, the particles undergo sintering as the calcination time is increased. The net effect is grain growth, particle coarsening and decreased surface area. Nanoparticles are especially sensitive to increases in temperature and calcination time leading to a rapid increase in particle size and the formation of μm-sized particles.

ZnO is normally a white, finely divided material with wurtzite structure. In this study, however, the resulting powders were slightly yellow owing to the evaporation of oxygen from the lattice to give a non-stoichiometric phase $Zn_{1+x}O$ (x typically $\leqslant 70$ ppm) on heating. After calcination, the particle size of the resulting powders was 20 nm (pH 10, $NH_2CO_2NH_4$). The specific surface area was 98 $m^2\,g^{-1}$ as determined by the BET method. The density of the powders was 3.45 $g\,cm^{-3}$ for precipitates before calcination and 4.95 $g\,cm^{-3}$ for ZnO powders obtained after calcination.

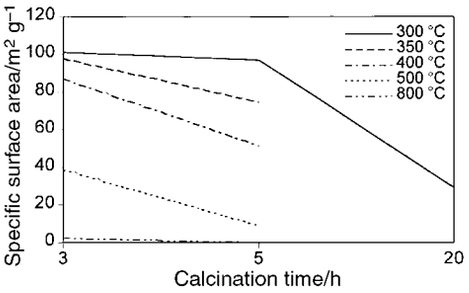

Fig. 18 The specific surface area of the zinc oxide precursor calcined at different temperatures and different calcination times.

Conclusions

The chemical precipitation method has been used for the synthesis of ZnO nanoparticles with controlled morphology. In the present study, ammonium carbamate was used as a precipitating reagent, which also affected the particle size and contributed to the formation of unusual rod morphology. A moderate ammonia concentration was beneficial in limiting the particle growth. Ultrafine particles, *ca.* 20 nm in size, could be obtained. Using the FIS technique it is possible to prepare a uniform powder with a particle size smaller than that obtained for the synthesis of powders from solution under the same conditions. Compared with conventional solution methods, this technique avoids large concentration gradients and gives better control of the particle growth in chemical processing systems. As precipitation is carried out at a low concentration, agglomeration is reduced, while when the reactant concentration is high, a high particle number density results and agglomeration is observed.

Acknowledgements

This work is supported by funds from the Consortium on Clusters and Ultrafine Particles.

References

1 A. S. Perl, *Am. Ceram. Soc. Bull.*, 1990, **74**, 780.
2 H. Rensmo, K. Keis, H. Lindström, S. Södergren, A. Solbrand, A. Hagfeldt, S.-E. Lindquist, L. N. Wang and M. Muhammed, *J. Phys. Chem. B*, 1997, **101**, 2598.
3 H. E. Brown, *Zinc oxide*, International Lead Zinc Research Organization, Inc., New York, NY, 1976.
4 M. S. El-Shall, D. Graiver and U. Pernisz, *NanoStruct. Mater.*, 1995, **6**, 297.
5 M. Muhammed, *Analusis*, 1996, **24**, M12.
6 T. Liu, O. Sakurai, N. Mizutani and M. Kato, *J. Mater. Sci.*, 1986, **21**, 3698.
7 G. Westin and M. Nygren, *J. Mater. Sci.*, 1992, **27**, 1617.
8 G. Westin, Å. Ekstrand, M. Nygren, R. Österlund and P. Merkelbach, *J. Mater. Chem.*, 1994, **4**, 615.
9 E. A. Meulenkamp, *J. Phys. Chem. B*, 1998, **102**, 5566.
10 B. Chiou, Y. J. Tsai and J. Duh, *J. Mater. Sci. Lett.*, 1988, **7**, 785.
11 A. Packter and A. Derry, *Cryst. Res. Technol.*, 1986, **21**, 1281.
12 M. E. V. Costa and J. L. Baptista, *J. Eur. Ceram. Soc.*, 1993, **11**, 275.
13 T. Baird, K. C. Campbell, P. J. Holliman, R. W. Hoyle, D. Stirling, B. P. Williams and M. Morris, *J. Mater. Chem.*, 1997, **7**, 319.
14 L. N. Wang, Y. Zhang and M. Muhammed, *J. Mater. Chem.*, 1995, **5**, 309.
15 P. Ayyub, *Indian J. Pure Appl. Phys.*, 1994, **32**, 611.
16 L. T. Skeggs, *Anal. Chem.*, 1966, **38**, 31A.
17 E. H. Hansen and J. Ruzicka, *J. Chem. Educ.*, 1979, **56**, 677.
18 M. F. Gine, H. Bergamin, E. A. G. Zagatto and B. F. Reis, *Anal. Chem. Acta*, 1980, **114**, 191.
19 N. N. Greenwood and A. Earnshaw, *Chemistry of the Elements*, Pergamon, Oxford, 1984, p. 1403.
20 P. Schindler, M. Reinert and H. Gamsjäger, *Helv. Chim. Acta*, 1969, **52**, 2327.

21 F. A. Carey, *Organic Chemistry*, McGraw-Hill, New York, 2nd edn., 1992, p. 832.
22 K. G. Tiller and J. G. Pickering, *Clays Clay Miner.*, 1974, **22**, 409.
23 G. Socrates, *Infrared Characteristic Group Frequencies*, Wiley, Chichester, 1980, p. 207.
24 K. Nakamoto, *Infrared Spectra of Inorganic and Coordination Compounds*, Wiley, New York, 1963, p. 169.
25 F. G. Sherif and F. A. Via, *US Pat.*, 4 764 357, 1988, to Akzo America Inc.

Paper 9/07098B